

# Quantitative Analysis of Neuronal Mitochondrial Movement Reveals Patterns Resulting from Neurotoxicity of Rotenone and 6-hydroxydopamine

**Rui F. Simões**

CNC, Center for Neuroscience and Cell Biology, UC Biotech, Biocant Park, 3060-197 Cantanhede, Portugal

**Rute Pino**

CISUC, Department of Informatics Engineering, University of Coimbra, 3030 Coimbra, Portugal

**Maurício Moreira-Soares**

OCBE, Faculty of Medicine, University of Oslo, Oslo, Norway

**Jaromira Kovarova**

Institute of Biotechnology, Czech Academy of Sciences, 252 50 Prague-West, Czech Republic

**Jiri Neuzil**

Institute of Biotechnology, Czech Academy of Sciences, 252 50 Prague-West, Czech Republic

**Rui Travasso**

CFisUC, Department of Physics, University of Coimbra, 3004-516 Coimbra, Portugal

**Paulo J. Oliveira**

CNC, Center for Neuroscience and Cell Biology, UC Biotech, Biocant Park, 3060-197 Cantanhede, Portugal

**Teresa Cunha-Oliveira** (✉ [teresa.oliveira@uc-biotech.pt](mailto:teresa.oliveira@uc-biotech.pt))

CNC, Center for Neuroscience and Cell Biology, UC Biotech, Biocant Park, 3060-197 Cantanhede, Portugal

**Francisco B. Pereira**

CISUC, Department of Informatics Engineering, University of Coimbra, 3030 Coimbra, Portugal

---

## Research Article

**Keywords:** Live cell imaging, Mitochondria movement, Trajectory descriptors, Neurotoxicants, Exploratory data analysis, Principal component analysis

**Posted Date:** March 17th, 2021

**DOI:** <https://doi.org/10.21203/rs.3.rs-296431/v1>

**License:**  This work is licensed under a Creative Commons Attribution 4.0 International License.

[Read Full License](#)

---

**Version of Record:** A version of this preprint was published at The FASEB Journal on November 9th, 2021.

See the published version at <https://doi.org/10.1096/fj.202100899R>.

**Quantitative analysis of neuronal mitochondrial movement reveals patterns  
resulting from neurotoxicity of rotenone and 6-hydroxydopamine**

Authors: Rui F. Simões<sup>1</sup>, Rute Pino<sup>2</sup>, Maurício Moreira-Soares<sup>3,4</sup>, Jaromira Kovarova<sup>5</sup>,  
Jiri Neuzil<sup>5,6</sup>, Rui Travasso<sup>7</sup>, Paulo J. Oliveira<sup>1</sup>, Teresa Cunha-Oliveira<sup>1,\*</sup>, Francisco B.  
Pereira<sup>2,8</sup>

Affiliations:

1 - CNC, Center for Neuroscience and Cell Biology, UC Biotech, Biocant Park, 3060-197  
Cantanhede, Portugal

2 - CISUC, Department of Informatics Engineering, University of Coimbra, 3030 Coimbra,  
Portugal

3 - OCBE, Faculty of Medicine, University of Oslo, Oslo, Norway

4 - Centre for Bioinformatics, Faculty of Mathematics and Natural Sciences, University of Oslo,  
Oslo, Norway

5 - Institute of Biotechnology, Czech Academy of Sciences, 252 50 Prague-West, Czech  
Republic

6 - School of Medical Science, Griffith University, Southport, 4222 Qld, Australia

7 - CFisUC, Department of Physics, University of Coimbra, 3004-516 Coimbra, Portugal

8 - Coimbra Polytechnic - ISEC, 3030-190 Coimbra, Portugal

\*Corresponding author:

#Teresa Cunha-Oliveira, MitoXT (Mitochondrial Toxicology and Experimental Therapeutics  
Laboratory), CNC, Center for Neuroscience and Cell Biology, UC Biotech Building (Lote 8A),  
Biocant Park, 3060-197 Cantanhede, Portugal; phone: +351 231249170 (ext 715); fax: +351  
231249179; email: teresa.oliveira@uc-biotech.pt; teresa.oliveira@gmail.com

**Keywords:** Live cell imaging; Mitochondria movement; Trajectory descriptors; Neurotoxicants; Exploratory data analysis; Principal component analysis.

**Abbreviations:** 6-OHDA, 6-hydroxydopamine; ATP, adenosine triphosphate; BSA, bovine serum albumin;  $\text{Ca}^{2+}$ , calcium; fps, frames per second; MIRO, mitochondrial rho; PCA, Principal Component Analysis; PBS, phosphate buffer saline; RA, retinoic Acid; TIRF, Total internal reflection fluorescence; TRAK, trafficking kinesin-binding.

## **Abstract**

Alterations in mitochondrial dynamics, including their intracellular trafficking, are common early manifestations of neuronal degeneration. However, current methodologies used to study mitochondrial trafficking events rely on parameters that are mostly altered in later stages of neurodegeneration. Our objective was to establish a reliable computational methodology to detect early alterations in neuronal mitochondrial trafficking. We propose a novel quantitative analysis of mitochondria trajectories based on innovative movement descriptors, including straightness, efficiency, anisotropy, and kurtosis. Using biological data from differentiated SH-SY5Y cells treated with the mitochondrial toxicants 6-hydroxydopamine and rotenone, we evaluated time- and dose-dependent alterations in trajectory descriptors. MitoTracker Red CMXRos-labelled mitochondria movement was analyzed by total internal reflection fluorescence microscopy followed by computational modelling to describe the process. This innovative analysis of mitochondria trajectories, based on the aforementioned trajectory descriptors, provides insights into mitochondrial movement characteristics and can be a consistent and sensitive method to detect alterations in mitochondrial trafficking occurring in the earliest time points of neurodegeneration.

## 1. Introduction

Neurons are polarized post-mitotic cells encompassing three structurally, functionally, and metabolically distinct domains, i.e. the cell body, dendrites with numerous branches, and the axon. These domains display unique metabolic and energetic needs, and they rely on mitochondrial adenosine triphosphate (ATP) production to accomplish their specific functions<sup>1-3</sup>. Mitochondria-produced ATP is vital for neuronal cell growth and survival, synapse formation and assembly, generation of action potentials, synaptic transmission and synaptic vesicle trafficking<sup>4-6</sup>. Additionally, mitochondria are also pivotal in calcium ( $\text{Ca}^{2+}$ ) homeostasis in neuronal cells, buffering transient  $\text{Ca}^{2+}$  levels by its sequestration and release, as needed<sup>7,8</sup>. As individual neuronal domains feature specific needs for the level of  $\text{Ca}^{2+}$  as well as metabolites, their homeostasis is maintained by corresponding number of mitochondria<sup>1,9,10</sup>.

Due to their morphological and metabolic characteristics, neuronal cells have developed mechanisms to transport mitochondria along microtubular tracks. The movement from the cell body to cellular extremities (anterograde transport) is mediated by the kinesin-1 family proteins, while dynein proteins are responsible for the opposite movement (retrograde transport). Both types of transport are dependent on ATP hydrolysis<sup>11,12</sup>. Movement of mitochondria is dependent on the polarity of microtubules, polymeric structures composed of  $\alpha$ - and  $\beta$ - tubulin, that polymerize from the minus to the plus end. In axons, the minus end is directed towards the cell body and the plus end to the cell extremity<sup>13,14</sup>. Thus, kinesins carry mitochondria from the minus to the plus end and dyneins from the plus to the minus end<sup>15</sup>.

Mitochondrial trafficking is also dependent on adaptor proteins, which ensure targeted and efficient transport regulation. The trafficking kinesin-binding (TRAK) proteins 1 and 2 bridge the mitochondrial rho (MIRO) 1 and 2 proteins and kinesins to control

mitochondrial anterograde trafficking<sup>16,17</sup>. Relevant for the retrograde transport, dynactin binds to dynein and to the microtubules, enhancing dynein motor processivity<sup>11,18</sup>. Mitochondrial docking processes allow mitochondria to remain stationary in areas with elevated ATP demand and Ca<sup>2+</sup> buffering dependency<sup>1</sup>. It has been described that between 10% and 40% of mitochondria in a neuronal cell are in motion, while 60% to 90% of the organelles are stationary<sup>10,19,20</sup>.

Since mitochondria are physically allocated to areas with higher metabolic activity and also based on regulation of Ca<sup>2+</sup> homeostasis, aberrations in mitochondrial dynamics, metabolism and mobility, leading to altered ATP production and lower Ca<sup>2+</sup> buffering capacity, are involved in the development of neurodegenerative pathologies, such as Alzheimer's disease, Huntington's disease, Parkinson's disease, and amyotrophic lateral sclerosis<sup>1</sup>. Furthermore, it was previously shown that alterations in mitochondrial motility appear prior to the first signs of neurodegeneration (such as degeneration of axons and cell death)<sup>21,22</sup>.

Mitochondria move along short or long paths with varying velocities and directions, often altering those parameters as a response to different stimuli<sup>23</sup>. Additionally, mitochondria undergo morphological alterations during movement, posing an increased challenge in the identification and segmentation of individual mitochondria. A further obstacle is the low signal-to-noise ratio of many microscopic approaches, yielding poor quality images<sup>24</sup>. Associated video acquisition processes can be detrimental due to photobleaching and phototoxicity<sup>25</sup>. Therefore, the videos taken under these microscopy approaches are either short (2-5 min) with 1-2 frames per second (fps)<sup>20,24,26</sup> or longer (30 min) but with 1 frame every 5-10 s<sup>27</sup>. Short videos cannot collect all features required to characterize mitochondrial motion while in longer movies, important information may be lost between frames.

To circumvent the limitations described, we used here total internal reflection fluorescence (TIRF) microscopy that takes advantage of a special mode of sample illumination, exciting only fluorophores located near the sample interface (about 100 nm), without exciting sample regions located further away. Images obtained with this microscopy technique present higher signal-to-noise ratio and almost nonexistent out-of-focus fluorescence, preventing photobleaching and phototoxicity<sup>28-30</sup>.

We exposed the cells to mitochondrial toxins, evaluated the mitochondrial movement by TIRF microscopy, and used computer modelling to describe the process. Our results present a new quantitative paradigm of mitochondrial dynamics in health and diseased neuronal cells.

## **2. Results**

### **2.1. 6-OHDA and rotenone decreased ATP levels in a concentration and time-dependent manner.**

Mitochondrial trafficking in neuronal cells is highly dependent on ATP consumption, since kinesin and dynein transport requires ATP hydrolysis (Hirokawa et al. 2010). We initially measured cellular ATP levels after treating cells for 24 h and 96 h with 6-OHDA (Supplementary Fig. S1 a) and rotenone (Supplementary Fig. S1 b). While there was little if any effect of the agents at 24 h, 96h-treatment caused significant decrease ( $p < 0.05$ ) in ATP levels (Supplementary Fig. S1).

### **2.2. 6-OHDA and rotenone reduced the level of $\beta$ III tubulin.**

We next tested the effect of 6-OHDA and rotenone on tubulin levels in differentiated SH-SY5Y cells. All 6-OHDA treatments (except 12.5  $\mu$ M for 96 h) significantly decreased



( $p < 0.05$ ) the levels of tubulin (Supplementary Fig. S2 a and b). Regarding rotenone, 125 nM and 250 nM for the 24-h time point induced an evident decreased ( $p = 0.02$  for both treatments) in tubulin levels (Supplementary Fig. S2 c). This effect was considerably stronger for the 96-h treatment (Supplementary Fig. S2 d). Representative images of cells treated with different concentrations of 6-OHDA (ii-v) and rotenone (vi-ix) for 24 h (e) and 96 h (f) are shown in Supplementary Fig. S2 e and f.

### 2.3. Mitochondrial net displacement is decreased by treatment with 6-OHDA and rotenone.

Treatment with 50  $\mu\text{M}$  6-OHDA for 24 h resulted in significantly smaller ( $p = 0.04$ ) mitochondrial net displacement. When incubated for 96 h, all 6-OHDA concentrations substantially decreased ( $p < 0.004$ ) mitochondrial net displacement in differentiated SH-SY5Y cells when compared to their control counterparts (Fig 1 a). Incubation with 62.5 nM rotenone for 24 h resulted, on average, in a 22% reduction of mitochondria net displacement ( $p = 0.06$ ), reaching statistical significance at 125 and 250 nM ( $p = 0.002$  and  $p = 0.003$ , respectively). Cells treated for 96 h with rotenone presented a significant decrease ( $p < 0.04$ ) in mitochondrial net displacement when compared to untreated counterparts (Fig 1 b).

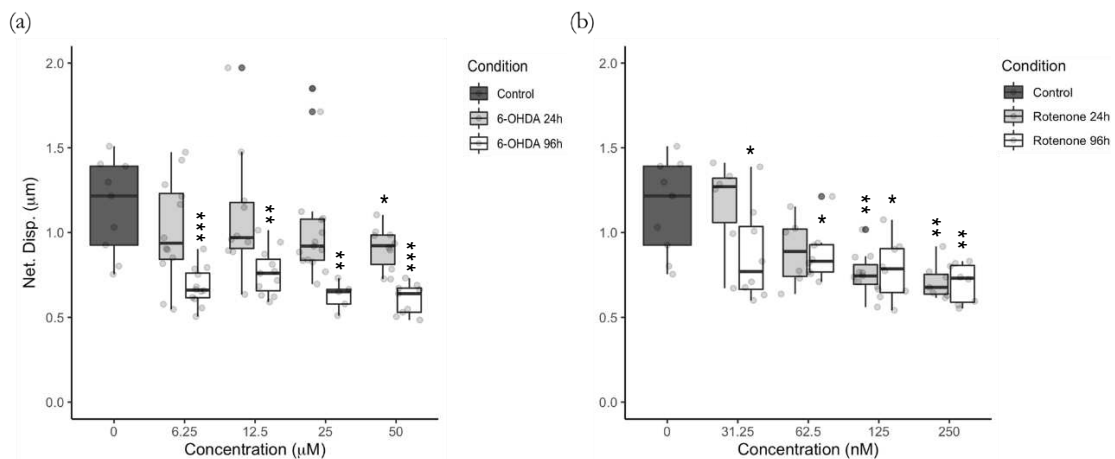


**Fig 1 – 6-OHDA (a) and rotenone (b) reduced mitochondrial net displacement.**

Mitochondria were labeled with the fluorescent dye MitoTracker Red CMXRos, their movement followed, and trajectory net displacement was calculated as stated in Materials and Methods. Data are presented as boxplots, in which each dot represents the mean of each mitochondrial movement per video frame (n=5 to 15). Kruskal-Wallis test (one-way ANOVA on ranks) pair-wise (control vs 6-OHDA or control vs rotenone) was used to assess statistical significance, (\*\*\*)  $p < 0.001$  (\*\*),  $p < 0.01$ , (\*)  $p < 0.05$ .

#### **2.4. Mitochondrial mean velocity is decreased by treatment with 6-OHDA and rotenone.**

Our results indicated that mitochondria move in control cells with the rate of 0.1 to 0.6  $\mu\text{m/s}$ . (Fig 2 a). Differentiated SH-SY5Y cells treated with 6-OHDA for 24 h exhibited a significant decrease in mitochondria mean velocity when incubated with 25  $\mu\text{M}$  and 50  $\mu\text{M}$  ( $p=0.04$  for both treatments). Cells incubated with 12.5  $\mu\text{M}$  ( $p=0.06$ ), 25  $\mu\text{M}$  ( $p=0.1$ ) and 50  $\mu\text{M}$  ( $p=0.09$ ) 6-OHDA for 96 h showed mitochondrial movement, on average, 55% slower than mitochondria in untreated cells, reaching statistical significance ( $p=0.04$ ) when treated with 6.25  $\mu\text{M}$  (Fig 2 a). Rotenone-treated cells incubated with 125 nM ( $p=0.07$ ) and 250 nM ( $p=0.08$ ) for 96 h revealed 55% slowed movement of mitochondria, although this did not reach significance (Fig 2 b).

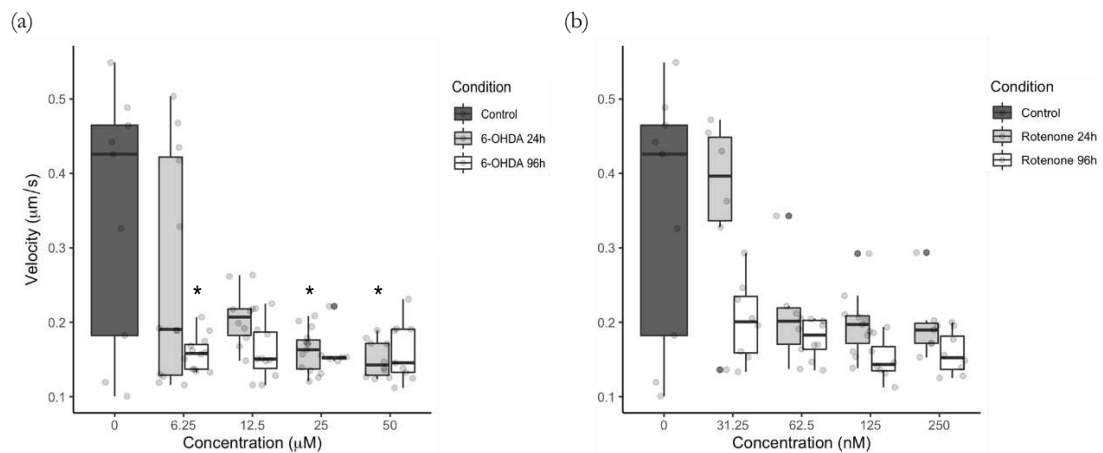


**Fig 2 – Mitochondrial mean velocity is lower due to 6-OHDA (a) and rotenone (b) treatment.**

Mitochondria were labeled with the fluorescent dye MitoTracker Red CMXRos, their movement followed, and trajectory mean velocity was calculated as stated in Materials and Methods. Data are presented as boxplots in which each dot represents the mean of each mitochondrial movement per video frame (n=5 to 15). Kruskal-Wallis test (One-way ANOVA on ranks) pair-wise (control vs 6-OHDA or control vs rotenone) was used to assess statistical significance, (\*) p< 0.05.

## 2.5. Mitochondrial movement trajectory is affected by 6-OHDA and rotenone.

Concerning mitochondria trajectory straightness, mitochondria in cells treated for 24 h with 50  $\mu\text{M}$  6-OHDA showed non-straight movement trajectories when compared to control cells (p=0.03). The other concentrations of 6-OHDA caused only minor alteration of mitochondrial movement trajectories (Fig 3 a). Rotenone at 125 nM induced a 17% decrease in mitochondria trajectory straightness although this was not significantly different from parental cells (p=0.07). No alterations were found for the other rotenone concentrations (Fig 3 b).

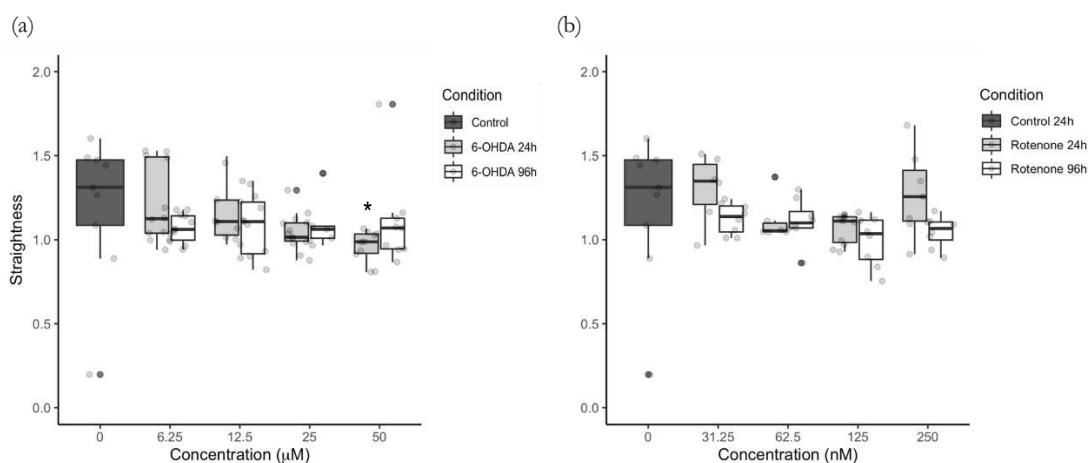


**Fig 3 – Mitochondrial movement pattern straightness was affected in cells treated with 6-OHDA (a) and rotenone (b).**

Mitochondria were labeled with the fluorescent dye MitoTracker Red CMXRos, their movement followed, and trajectory straightness was calculated as stated in Materials and Methods. Data are presented as boxplots in which each dot represents the mean of each mitochondria movement per video frame (n=5 to

15). Kruskal-Wallis test (One-way ANOVA on ranks) pair-wise (control vs 6-OHDA or control vs rotenone) was used to assess statistical significance, (\*)  $p < 0.05$ .

Regarding individual mitochondria, the trajectory efficiency was small even in control cells (0.2 to 0.4) (Fig 4 a and b). Cells treated for 96 h with 6.25  $\mu\text{M}$  ( $p=0.06$ ), 12.5  $\mu\text{M}$  ( $p=0.1$ ), 25  $\mu\text{M}$  ( $p=0.07$ ) and 50  $\mu\text{M}$  ( $p=0.06$ ) 6-OHDA showed, on average, a decrease in 17%, 13%, 24% and 21%, respectively, in mitochondrial trajectory efficiency. Regarding cells treated for 24 h, the highest 6-OHDA concentration (50  $\mu\text{M}$ ) resulted in a 17% average decrease in mitochondria trajectory efficiency ( $p=0.07$ ) (Fig 4 a). Treatment with 62.5 nM for 24 h ( $p=0.09$ ) and with 125 nM rotenone (both 24 h and 96 h,  $p=0.06$  for both treatments) displayed an average 15%, 21% and 21% decrease of mitochondrial trajectory efficiency when compared to control cells (Fig 4 b).

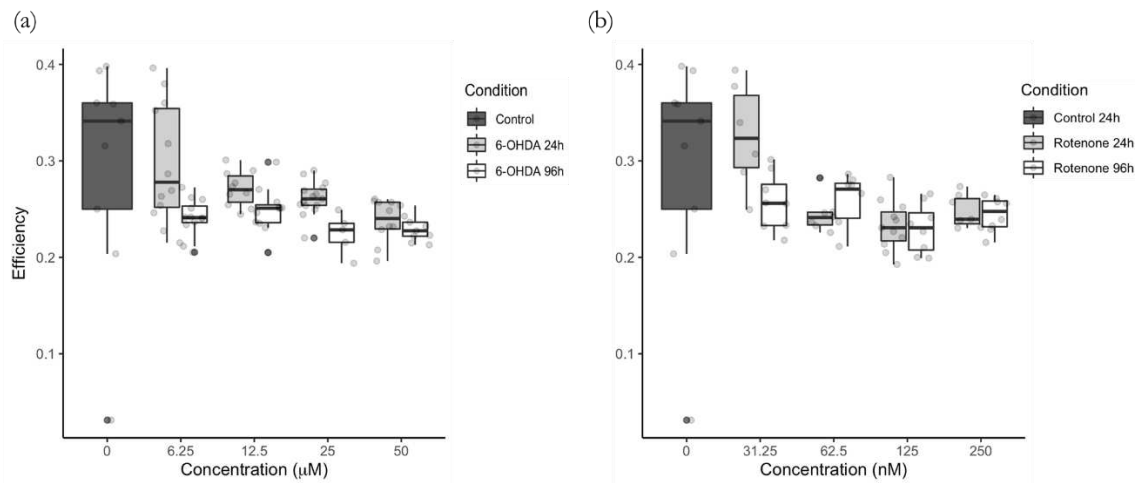


**Fig 4 – Mitochondrial trajectory efficiency was decreased in cells treated with 6-OHDA (a) and with rotenone (b).**

Mitochondria were labeled with the fluorescent dye MitoTracker Red CMXRos, their movement followed, and trajectory efficiency was calculated as stated in Materials and Methods. Data are represented as boxplots in which each dot represents the mean of each mitochondria movement per video frame ( $n=5$  to 15). Kruskal-Wallis test (One-way ANOVA on ranks) pair-wise (control vs 6-OHDA or control vs rotenone) was used to assess statistical significance.

## 2.6. Mitochondria in cells treated with 6-OHDA and rotenone exhibit a higher degree of trajectory anisotropy.

Cells incubated for 24 h and 96 h with 6-OHDA at all concentrations, with the exception of the highest concentration (50  $\mu\text{M}$ ) for both time points, showed a significant increase ( $p < 0.04$ ) in mitochondrial trajectory anisotropy, which was reflected by more unidimensional trajectories (Fig 5 a). Regarding rotenone, the profile was different in 24 h treated cells. Mitochondria in cells incubated for 96 h with the lower rotenone concentrations, 31.25 nM and 62.5 nM, showed significantly higher degree of trajectory anisotropy ( $p = 0.002$  and  $p = 0.05$ , respectively), exhibiting a more unidimensional trajectory. However, cells treated for 24 h with rotenone at 62.5 nM ( $p = 0.03$ ) and 250 nM ( $p = 0.007$ ) of rotenone showed a significant elevation of the degree of mitochondrial trajectory anisotropy (Fig 5 b).

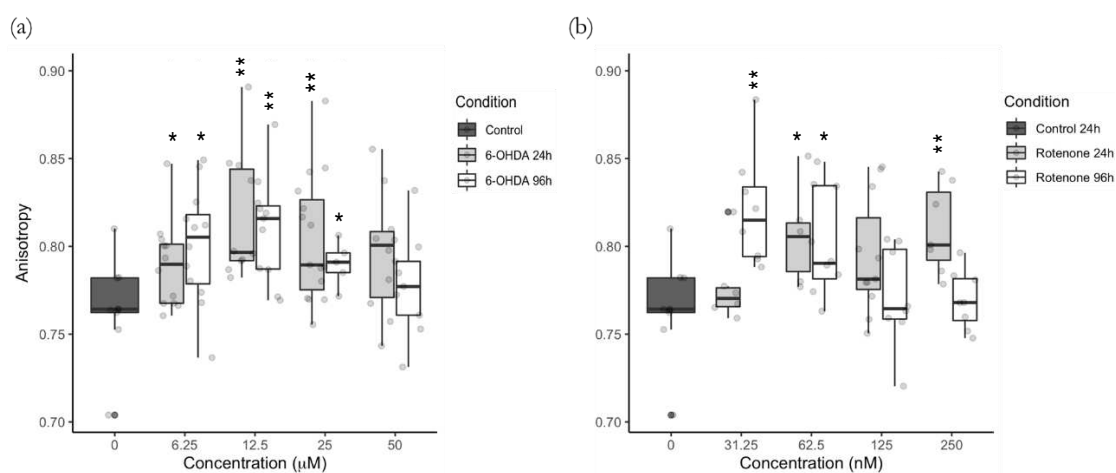


**Fig 5 – 6-OHDA (a) and rotenone (b) promote higher degree of mitochondrial movement anisotropy.**

Mitochondria were labeled with the fluorescent dye MitoTracker Red CMXRos, their movement followed, and trajectory anisotropy was calculated as stated in Materials and Methods. Data are represented as boxplots in which each dot represents the mean of each mitochondria movement per video frame ( $n = 5$  to 15). Kruskal-Wallis test (One-way ANOVA on ranks) pair-wise (control vs 6-OHDA or control vs rotenone) was used to assess statistical significance, (\*\*),  $p < 0.01$ , (\*)  $p < 0.05$ .

## 2.7. Shorter incubation times with 6-OHDA enhance kurtosis of mitochondrial movement pattern.

Significant increase of mitochondrial trajectory kurtosis was observed in cells treated for 24 h with the with 6-OHDA at 25  $\mu\text{M}$  and 50  $\mu\text{M}$  ( $p=0.04$  for both concentrations) (Fig 6 a). On the other hand, no changes in kurtosis were observed for cells treated with 6-OHDA at the lower concentrations (Fig 6 a) and with rotenone at all concentrations (Fig 6 b).

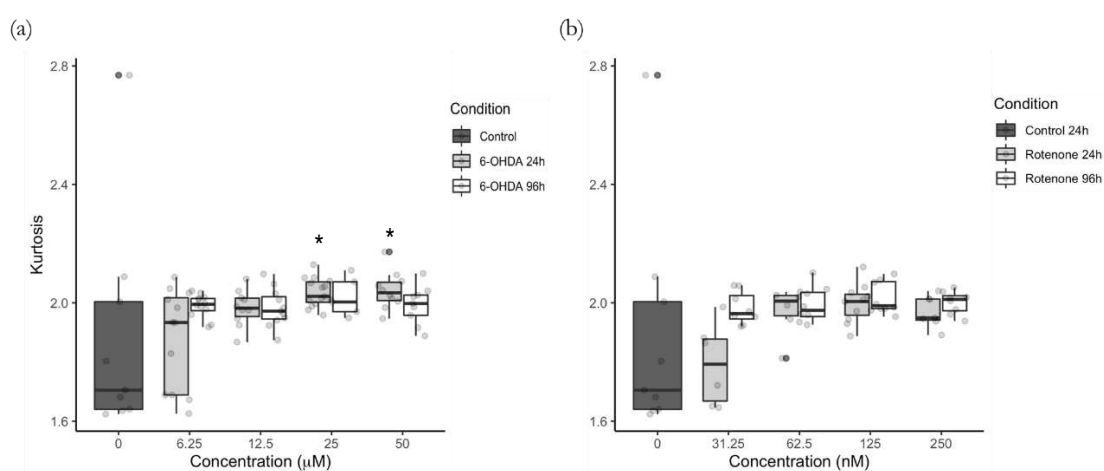


**Fig 6 – Kurtosis of mitochondrial movement and the effect of 6-OHDA (a) and rotenone (b).**

Mitochondria were labeled with the fluorescent dye MitoTracker Red CMXRos, their movement followed, and trajectory kurtosis was calculated as stated in Materials and Methods. Data are represented as boxplots in which each dot represents the mean of each mitochondria movement per video frame ( $n=5$  to 15). Kruskal-Wallis test (One-way ANOVA on ranks) pair-wise (control vs 6-OHDA or control vs rotenone) was used to assess statistical significance, (\*)  $p < 0.05$ .

## 2.8. Principal component analysis distinguishes control and treated cells.

We performed PCA using the R stats library. The data were zero-centered and scaled to obtain unit variance before the analysis (z-score normalization)<sup>31</sup>. In Fig 7, we show the PCA evaluation with the ellipses centered at the mean vector of the data points, which

provide a visual intuition of the covariance<sup>32</sup>. Treatments with 6-OHDA for 24 h presents a significant separation from the control (with variances of 62.2% and 37.8%), except for the lowest concentration (6.25  $\mu$ M), at which the cluster shows a considerable superposition with control (Fig 7 a). The same pattern was observed for cells treated with rotenone for 24 h (with variances of 63.4% and 36.6%), in which the treatments data formed distinct clusters when compared to the control ones. However, the PCA shows essentially no difference between the control cells and those treated with 31.25 nM rotenone. For higher concentrations, a clockwise rotation of the principal axes with relation to control was observed, with higher variance along the anisotropy direction (Fig 7 b). In addition, for 96 h treatments with 6-OHDA (with variances 59.9% and 40.1%) (Fig 7 c) or rotenone (with variances 52.4% and 47.6%) (Fig 7 d), we observed that the results were grouped far from the control, indicating that a longer period of treatment may overcome the weak effect associated with lower concentrations. The data ellipses showed a trend for a covariance decrease as the concentration of 6-OHDA and rotenone increase for the 96 h treatments.

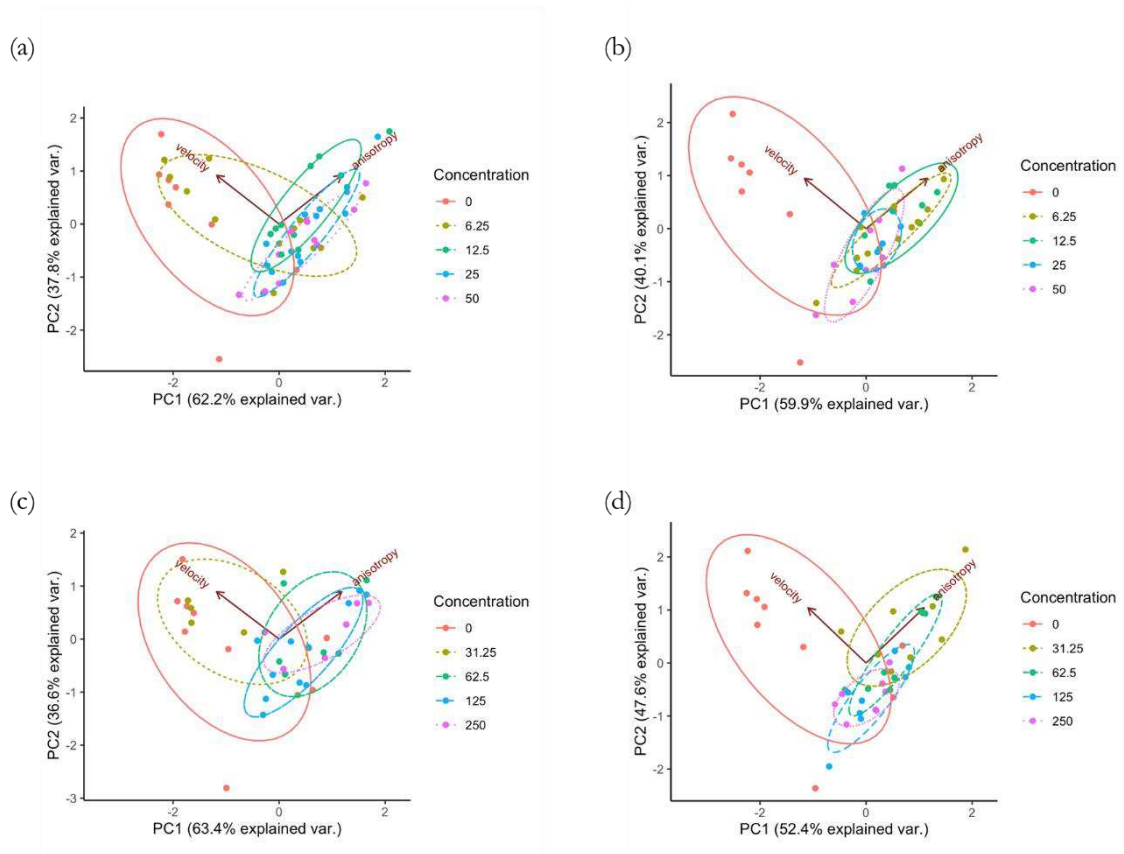


**Fig 7 – The panel shows PCAs for control together with each different treatment: 6-OHDA for 24 h (a) and 96 h (b) and rotenone for 24 h (c) and 96 h (d).**

The normal data ellipses are superposed. Only the two best features that better distinguish between the treatments and control conditions were considered, i.e. velocity and anisotropy. In general, the treatments grouped far from the control and presented higher variance along the anisotropy direction, apart from the treatments for 24 h with lowest concentration of 6-OHDA and rotenone.



### 3. Discussion

In recent years, the improvement of microscopy methods (enabling the acquisition of high signal-to-noise images) together with the development of automated particle tracking algorithms with certain level of accuracy allowed for the analysis of mitochondrial motility. However, a very careful and critical analysis should be performed when evaluating mitochondrial trafficking. A prime example is the study of mitochondrial mean velocity. It has been demonstrated that, depending on the cell model as well as method of mitochondrial tracking and movement analysis, the values of this parameter could range from an average of 0.1  $\mu\text{m/s}$  to 1.5  $\mu\text{m/s}$  <sup>20,21,23,33</sup>. To the best of our knowledge, no studies of mitochondrial trafficking have been performed using SH-SY5Y cells. Since we found that the rate of mitochondrial movement using these cells is 0.1-0.6  $\mu\text{m/s}$ , SH-SY5Y cells present a plausible model for these studies.

In order to provide novel insights into mitochondria trajectory analysis and efficiency, we treated differentiated SH-SY5Y cells with 6-OHDA or rotenone and performed a more detailed analysis than carried out in previous studies presented in the literature. A key enhancement of our approach is the adoption of a wider range of features that help to characterize mitochondrial trajectories (such as their anisotropy, kurtosis, straightness and efficiency). A similar approach has been previously applied to the study of human natural killer cell migration in culture <sup>34</sup> and diffusion of nanoparticles in cellular microenvironment <sup>35</sup>.

6-OHDA is a neurotoxic agent known to disrupt mitochondrial trafficking <sup>36,37</sup>. This substance is a hydroxylated analogue of the neurotransmitter dopamine <sup>38</sup> that induces mitochondrial toxicity by inhibiting complex I function, ensuing in superoxide production <sup>39</sup>. 6-OHDA can also inhibit complex IV <sup>40</sup>. Cells treated with 6-OHDA for 96 h exhibited

a more indirect and less efficient trajectory featuring higher anisotropy. This may be explained by the negative synergistic effect of a significant decrease in ATP level and the level of  $\beta$ III tubulin. Thus, 6-OHDA alters cell bioenergetics and microtubular tracks that are both indispensable for mitochondrial movement, ultimately resulting in a strong effect on dynamics of mitochondrial trafficking. Mitochondria trajectories in cells treated with this compound for 24 h presented, for higher concentrations (25  $\mu$ M and 50  $\mu$ M), a decrease in straightness, efficiency and net displacement but an increase in kurtosis. This weaker effect at shorter treatment times is possibly due to a smaller impact in reducing ATP levels.

Changes in mitochondrial trafficking have been described in cells treated with 6-OHDA. In a study using Lund human mesencephalic cells treated with 6-OHDA at 40  $\mu$ M, 100  $\mu$ M and 250  $\mu$ M for 4 h and 7 h showed a decrease in the number of mitochondria moving both in the anterograde and retrograde direction without affecting the rate of mitochondrial movement<sup>37</sup>. Similarly, it was shown that treatment with 60  $\mu$ M 6-OHDA for 30 min in dopaminergic neurons decreased mitochondrial motility by approximately 50%. Again, no velocity alteration was evident under this scenario<sup>36</sup>. Microtubule modifications and dynamics are also involved in 6-OHDA-related mitochondrial trafficking impairment. Related to our model, retinoic acid-differentiated SH-SY5Y cells treated with 30  $\mu$ M 6-OHDA showed tubulin acetylation, which resulted in decreased microtubule growth rate, and increased level of monomeric tubulin, suggesting tubulin depolymerization. This effect was attributed to oxidative modifications of molecules of tubulin<sup>41</sup>.

Rotenone is a time-dependent high-affinity irreversible inhibitor of complex I<sup>42-44</sup>. This compound leads to inhibition of oxidative phosphorylation and oxygen consumption, ultimately triggering a cellular bioenergetic deficit. This agent induces oxidative damage

of proteins, lipids and nucleic acids by means of generation of high levels of superoxide anion<sup>45-47</sup>. Rotenone-treated cells showed weaker effect, when compared to their 6-OHDA-treated counterparts, when assessing the trajectory properties, which are a focus of this study. Although ATP levels and the level of  $\beta$ III tubulin were decreased, no evident alterations were found in the trajectory straightness and kurtosis. Rotenone treatment, despite increasing anisotropy, indicated a more unidimensional trajectory and decreased trajectory efficiency.

Besides being involved in mitochondrial complex I inhibition, affecting ATP and superoxide anion production, neuronal cells treated with rotenone, both acutely and chronically, display alterations in mitochondrial trafficking. One study showed that primary cortical neurons acutely treated with 1  $\mu$ M rotenone exhibited an increase in the number of stationary mitochondria. Additionally, a significant decrease in the mean velocity of mitochondrial movement in both directions was also reported<sup>24</sup>. Using differentiated SH-SY5Y cells, it was shown that treatment of the cells with 50 nM rotenone for 8 and 16 days significantly suppressed the rate of mitochondrial trafficking. The authors hypothesized that the decrease in mitochondrial velocity was due to either the disruption of the microtubular network or oxidative stress<sup>48</sup>. Indeed, several studies have shown that rotenone destabilizes microtubules, inducing tubulin depolymerization. Dopaminergic neurons incubated with 100 nM rotenone for 30 min displayed a significant increase in free tubulin<sup>49</sup>. Additionally, incubation of cells with 10  $\mu$ M rotenone for 12 h induced microtubule depolymerization and blocked its re-polymerization in a similar cell model<sup>50</sup>. using non-neuronal cells, it was shown that rotenone induces tubulin conformational changes, affecting its secondary structure. This suppressed microtubule re-assembly and decreased the length of microtubules<sup>51</sup>.

Examining one of the most frequently analyzed features of mitochondrial movement, which is the mean velocity of mitochondria along tubulin tracks, together with a rarely assessed feature of mitochondrial mobility, i.e. the anisotropy of mitochondrial trajectories, we were able to clearly distinguish between cells treated with neuronal poisons epitomized by 6-OHDA and rotenone. This was particularly evident at the longer treatment times of 96 h. By considering mean velocity and anisotropy combined with the PCA projection, we observed that the dispersion in velocity decreases with the treatment while for anisotropy increases. This behavior was observed in retinoic acid-differentiated SHSY5Y cells treated with both agents, also presenting a tendency for decreased variance in anisotropy for longer treatments (96 h) and for higher concentrations of 6-OHDA (50  $\mu$ M) and rotenone (250 nM).

#### **4. Conclusion**

This study presents an innovative approach to quantitative analysis of mitochondria movement in differentiated SH-SY5Y cells treated with neuronal toxins at a range of concentrations and for different time points. Additionally to the conventionally studied movement characteristics such as mitochondrial net displacement and mean velocity, we introduced, for the first time, new movement descriptors to characterize mitochondria trajectories, i.e. their straightness, efficiency, anisotropy and kurtosis. We have demonstrated here for the first time that these new descriptors provide an insight into mitochondrial motility characteristics and can be used to characterize mitochondrial trajectories. Moreover, in cases in which mitochondrial length of movement and the movement duration, direction and velocity are not altered, these new trajectory

descriptors can present a reliable and sensitive method to detect, in particular, the initial stages of neuronal degeneration.

## **5. Material and methods**

### **5.1. Cell culture and treatments**

SH-SY5Y cells (ECACC, cat. 94030304) were cultured in supplemented Dulbecco's modified Eagle's medium (DMEM, D5030, Sigma-Aldrich, USA) and differentiated into a neuronal-like morphology following a protocol published by us<sup>52</sup>. Details are provided in the Supplementary methods section.

### **5.2. ATP levels determination**

Intracellular ATP was quantified using the CellTiter-Glo Luminescent Cell Viability Assay (G7570, Promega, USA) following manufacture's protocol. Details are provided in the Supplementary methods section.

### **5.3. Immunocytochemistry and fluorescence microscopy**

$\beta$ III tubulin (sc80005, Santa Cruz, Germany) levels and Hoechst 33342 (B2261, Sigma-Aldrich) nuclear labelling in fixed SH-SY5Y cells were assessed following the protocol described in the Supplementary methods section.

#### **5.4. Live cell imaging**

For live imaging, cells were differentiated in 35 mm  $\mu$ -dishes (81156, Ibidi Germany) at  $3 \times 10^4$  cells/cm<sup>2</sup> and treated with 6-OHDA and rotenone. Subsequently, mitochondria were stained with 25 nM of the mitochondrial fluorescent dye MitoTracker Red CMXRos (M7512, Invitrogen, Thermo Fisher Scientific) in the FluoroBrite DMEM Media (A1896702, Gibco, Thermo Fisher Scientific) for 30 min. The media was then replaced by fresh FluoroBrite DMEM Media. Movies of fluorescent mitochondria were then recorded using the TIRF-fitted Nikon Eclipse Ti2 inverted microscope. The lowest level of excitation light from the 561 nm laser was used for imaging, and the emitted light was collected using an mCherry filter. The EMCCD Andor iXon Ultra DU888 camera (Andor Technologies) was used to capture the images with resolution of 1024 x 1024 pixels (pixel size 13 x 13  $\mu$ m) at 1 frame per second for 10 min.

#### **5.5. Movie Processing**

Raw movie files were convolved and filtered using ImageJ. After applying noise reduction, they were saved as a sequence of binary images. A MATLAB algorithm ([www.github.com/kandelj/MitoSPT](http://www.github.com/kandelj/MitoSPT))<sup>53</sup> was then used to detect object movement across frames, allowing for the calculation of the trajectory, total and net distances traveled by each individual mitochondria. Movie processing details are provided in the Supplementary methods section.

## 5.6. Quantitative analysis of trajectories

Specific physical properties, describing the curve shape and kinematics of individual mitochondria trajectories, were obtained with the python package trajpy<sup>54,55</sup>, available at <https://github.com/ocbe-uio/trajpy/>. Supplementary figures 3-7 display some examples of trajectories. The calculated trajectory features are the following.

### 5.6.1. Mean velocity

We evaluated the mitochondria mean velocity  $\langle v \rangle$  by calculating the ratio between the total length of the trajectory and the elapsed time  $\Delta t$

$$\langle v \rangle = \frac{\sum_{i=1}^{N-1} |\mathbf{r}_{i+1} - \mathbf{r}_i|}{\Delta t}, \quad (1)$$

where  $N$  is the number of segments of the trajectory, and  $\mathbf{r}_i$  is the position of the  $i$ -th point along the trajectory path.

### 5.6.2. Anisotropy

The features related to the trajectory shape are functions of the gyration tensor obtained by the variance of the position along the trajectory. Mathematically, the components of the gyration tensor,  $R_{mn}$ , are given by the following equation:

$$R_{mn} = \frac{1}{2N^2} \sum_{i=1}^N \sum_{j=1}^N (r_{m,i} - r_{m,j}) (r_{n,i} - r_{n,j}), \quad (2)$$

in which  $m$  and  $n$  are indices for the coordinates along the directions  $x$ ,  $y$ ,  $z$ .

Using the diagonalized gyration tensor  $D$  to define the tensor,  $\hat{R} = D - 1/3(\text{Tr}D)\mathbb{1}$  with the unity tensor  $\mathbb{1}$ , we obtained the degree of anisotropy among the principal axes<sup>56</sup>, defined as

$$k^2 \equiv \frac{3}{2} \frac{Tr\hat{R}^2}{(Tr\hat{R})^2}, \quad (3)$$

where, the setting  $Tr\hat{R} = \lambda_1 + \lambda_2 + \lambda_3$ , gives

$$k^2 = 1 - 3 \frac{\lambda_1\lambda_2 + \lambda_2\lambda_3 + \lambda_3\lambda_1}{(\lambda_1 + \lambda_2 + \lambda_3)}, \quad (4)$$

The minimum anisotropy,  $k^2 = 0$ , is obtained when the distribution of the trajectory points is spherically symmetrical with  $\lambda_1 = \lambda_2 = \lambda_3$ . The maximum anisotropy,  $k^2 = 1$ , occurs when at least two eigenvalues are zero. High anisotropy refers to a small dimensionality in the principal axes coordinates - unidimensional trajectories present the highest anisotropy. Thus, anisotropy carries information about symmetry and dimensionality at the same time <sup>57</sup>.

### 5.6.3. Kurtosis

We obtained the kurtosis of the trajectory by projecting each position along the main principal eigenvector of the radius of the gyration tensor  $r_i^p = \mathbf{r}_i \cdot \mathbf{e}_{\lambda_1}$ , in which  $\mathbf{e}_{\lambda_1}$  is the eigenvector associated to the eigenvalue  $\lambda_1$ , and then calculating the quartic moment

$$K = \frac{1}{N} \sum_{i=1}^N \frac{(r_i^p - \langle r^p \rangle)^4}{\sigma_{r^p}^4}, \quad (5)$$

in which  $\langle r^p \rangle$  is the mean position of the projected trajectory and  $\sigma_{r^p}^2$  is its variance. Kurtosis is the measure of the ‘tailedness’ of the positions distribution in the trajectory <sup>58</sup>.

### 5.6.4. Straightness

Straightness compares the net displacement to the sum of displacements. It measures the likeliness of the trajectory to a straight line

$$S = \frac{|\mathbf{r}_N - \mathbf{r}_1|}{\sum_{i=1}^{N-1} |\mathbf{r}_{i+1} - \mathbf{r}_i|}, \quad (6)$$



where  $\mathbf{r}_1$  is the initial position and  $\mathbf{r}_N$  is the last position on the trajectory. If the trajectory is completely straight, the numerator and denominator are the same, consequently  $S = 1$ . On the other hand, if  $\sum_{i=1}^{N-1} |\mathbf{r}_{i+1} - \mathbf{r}_i| \gg \mathbf{r}_N - \mathbf{r}_1$ , then  $S \approx 0$ .

### 5.6.5. Efficiency

Efficiency is similar to straightness described above. It is defined as the ratio between the net displacement and the sum of squared displacements:

$$E_{ff} = \frac{|\mathbf{r}_N - \mathbf{r}_1|^2}{\sum_{i=1}^{N-1} |\mathbf{r}_{i+1} - \mathbf{r}_i|^2} \quad (7)$$

When a particle describes a long trajectory but ends at the same initial position, the measured efficiency will be zero. Moreover, for the same net displacement, a highly irregular trajectory will have smaller efficiency than the linear trajectory.

## **5.7. Statistics**

Data were analyzed using R 4.0.3<sup>31</sup>. Results are presented in boxplots (box-and-whisker plots), in which the middle line represents the median and the whiskers go down to the minimum value and up to the maximum value, where each individual value is represented as a data point. The number of experiments carried out is presented in the legend of the figures.

We performed the non-parametric Kruskal-Wallis test pair-wise comparisons between the control and each treatment condition followed by Dunn's post hoc for multiple conditions comparison. Statistical significance was set as (\*)  $p < 0.05$ , (\*\*)  $p < 0.01$ , (\*\*\*)  $p < 0.001$  and (\*\*\*\*)  $p < 0.0001$ . Principal component analysis (PCA) was employed to identify the underlying covariable patterns of the data.

## Data availability

The dataset generated during and/or analyzed during the current study are available on [https://figshare.com/projects/Quantitative\\_analysis\\_of\\_neuronal\\_mitochondrial\\_movement/99239](https://figshare.com/projects/Quantitative_analysis_of_neuronal_mitochondrial_movement/99239)

## References

- 1 Sheng, Z. H. & Cai, Q. Mitochondrial transport in neurons: impact on synaptic homeostasis and neurodegeneration. *Nat Rev Neurosci* **13**, 77-93, doi:10.1038/nrn3156 (2012).
- 2 Saxton, W. M. & Hollenbeck, P. J. The axonal transport of mitochondria. *J Cell Sci* **125**, 2095-2104, doi:10.1242/jcs.053850 (2012).
- 3 Sheng, Z. H. Mitochondrial trafficking and anchoring in neurons: New insight and implications. *J Cell Biol* **204**, 1087-1098, doi:10.1083/jcb.201312123 (2014).
- 4 Attwell, D. & Laughlin, S. B. An energy budget for signaling in the grey matter of the brain. *J Cereb Blood Flow Metab* **21**, 1133-1145, doi:10.1097/00004647-200110000-00001 (2001).
- 5 Harris, J. J., Jolivet, R. & Attwell, D. Synaptic energy use and supply. *Neuron* **75**, 762-777, doi:10.1016/j.neuron.2012.08.019 (2012).
- 6 Sun, T., Qiao, H., Pan, P. Y., Chen, Y. & Sheng, Z. H. Motile axonal mitochondria contribute to the variability of presynaptic strength. *Cell Rep* **4**, 413-419, doi:10.1016/j.celrep.2013.06.040 (2013).
- 7 Billups, B. & Forsythe, I. D. Presynaptic mitochondrial calcium sequestration influences transmission at mammalian central synapses. *J Neurosci* **22**, 5840-5847, doi:20026597 (2002).
- 8 Medler, K. & Gleason, E. L. Mitochondrial Ca(2+) buffering regulates synaptic transmission between retinal amacrine cells. *J Neurophysiol* **87**, 1426-1439, doi:10.1152/jn.00627.2001 (2002).
- 9 Schwarz, T. L. Mitochondrial trafficking in neurons. *Cold Spring Harb Perspect Biol* **5**, doi:10.1101/cshperspect.a011304 (2013).
- 10 Morris, R. L. & Hollenbeck, P. J. The regulation of bidirectional mitochondrial transport is coordinated with axonal outgrowth. *J Cell Sci* **104** ( Pt 3), 917-927 (1993).
- 11 Pilling, A. D., Horiuchi, D., Lively, C. M. & Saxton, W. M. Kinesin-1 and Dynein are the primary motors for fast transport of mitochondria in Drosophila motor axons. *Mol Biol Cell* **17**, 2057-2068, doi:10.1091/mbc.e05-06-0526 (2006).
- 12 Hirokawa, N., Niwa, S. & Tanaka, Y. Molecular motors in neurons: transport mechanisms and roles in brain function, development, and disease. *Neuron* **68**, 610-638, doi:10.1016/j.neuron.2010.09.039 (2010).
- 13 Kapitein, L. C. & Hoogenraad, C. C. Building the Neuronal Microtubule Cytoskeleton. *Neuron* **87**, 492-506, doi:10.1016/j.neuron.2015.05.046 (2015).
- 14 Nguyen, M. M., Stone, M. C. & Rolls, M. M. Microtubules are organized independently of the centrosome in Drosophila neurons. *Neural Dev* **6**, 38, doi:10.1186/1749-8104-6-38 (2011).
- 15 Yau, K. W. *et al.* Dendrites In Vitro and In Vivo Contain Microtubules of Opposite Polarity and Axon Formation Correlates with Uniform Plus-End-Out Microtubule Orientation. *J Neurosci* **36**, 1071-1085, doi:10.1523/JNEUROSCI.2430-15.2016 (2016).

- 16 MacAskill, A. F., Brickley, K., Stephenson, F. A. & Kittler, J. T. GTPase dependent recruitment of Grif-1 by Miro1 regulates mitochondrial trafficking in hippocampal neurons. *Mol Cell Neurosci* **40**, 301-312, doi:10.1016/j.mcn.2008.10.016 (2009).
- 17 Brickley, K. & Stephenson, F. A. Trafficking kinesin protein (TRAK)-mediated transport of mitochondria in axons of hippocampal neurons. *J Biol Chem* **286**, 18079-18092, doi:10.1074/jbc.M111.236018 (2011).
- 18 King, S. J. & Schroer, T. A. Dynactin increases the processivity of the cytoplasmic dynein motor. *Nat Cell Biol* **2**, 20-24, doi:10.1038/71338 (2000).
- 19 Ligon, L. A. & Steward, O. Movement of mitochondria in the axons and dendrites of cultured hippocampal neurons. *J Comp Neurol* **427**, 340-350, doi:10.1002/1096-9861(20001120)427:3<340::aid-cne2>3.0.co;2-y (2000).
- 20 Misgeld, T., Kerschensteiner, M., Bareyre, F. M., Burgess, R. W. & Lichtman, J. W. Imaging axonal transport of mitochondria in vivo. *Nat Methods* **4**, 559-561, doi:10.1038/nmeth1055 (2007).
- 21 Fang, C., Bourdette, D. & Banker, G. Oxidative stress inhibits axonal transport: implications for neurodegenerative diseases. *Mol Neurodegener* **7**, 29, doi:10.1186/1750-1326-7-29 (2012).
- 22 Bros, H., Millward, J. M., Paul, F., Niesner, R. & Infante-Duarte, C. Oxidative damage to mitochondria at the nodes of Ranvier precedes axon degeneration in ex vivo transected axons. *Exp Neurol* **261**, 127-135, doi:10.1016/j.expneurol.2014.06.018 (2014).
- 23 Bros, H., Hauser, A., Paul, F., Niesner, R. & Infante-Duarte, C. Assessing Mitochondrial Movement Within Neurons: Manual Versus Automated Tracking Methods. *Traffic* **16**, 906-917, doi:10.1111/tra.12291 (2015).
- 24 Chen, M. *et al.* A new method for quantifying mitochondrial axonal transport. *Protein Cell* **7**, 804-819, doi:10.1007/s13238-016-0268-3 (2016).
- 25 Coutu, D. L. & Schroeder, T. Probing cellular processes by long-term live imaging-- historic problems and current solutions. *J Cell Sci* **126**, 3805-3815, doi:10.1242/jcs.118349 (2013).
- 26 Gerencser, A. A. & Nicholls, D. G. Measurement of instantaneous velocity vectors of organelle transport: mitochondrial transport and bioenergetics in hippocampal neurons. *Biophys J* **95**, 3079-3099, doi:10.1529/biophysj.108.135657 (2008).
- 27 Chang, D. T., Rintoul, G. L., Pandipati, S. & Reynolds, I. J. Mutant huntingtin aggregates impair mitochondrial movement and trafficking in cortical neurons. *Neurobiol Dis* **22**, 388-400, doi:10.1016/j.nbd.2005.12.007 (2006).
- 28 Axelrod, D. Chapter 7: Total internal reflection fluorescence microscopy. *Methods Cell Biol* **89**, 169-221, doi:10.1016/S0091-679X(08)00607-9 (2008).
- 29 Mattheyses, A. L., Simon, S. M. & Rappoport, J. Z. Imaging with total internal reflection fluorescence microscopy for the cell biologist. *J Cell Sci* **123**, 3621-3628, doi:10.1242/jcs.056218 (2010).
- 30 Poulter, N. S., Pitkeathly, W. T., Smith, P. J. & Rappoport, J. Z. The physical basis of total internal reflection fluorescence (TIRF) microscopy and its cellular applications. *Methods Mol Biol* **1251**, 1-23, doi:10.1007/978-1-4939-2080-8\_1 (2015).
- 31 R Core Team. *R: A language and environment for statistical computing*. R Foundation for Statistical Computing. Vienna, Austria., <<http://www.r-project.org/index.html>> (2020).
- 32 Friendly, M., Monette, G. & Fox, J. Elliptical Insights: Understanding Statistical Methods through Elliptical Geometry. *Statist. Sci.* **28**, 1-39, doi:10.1214/12-STS402 (2013).
- 33 MacAskill, A. F. & Kittler, J. T. Control of mitochondrial transport and localization in neurons. *Trends Cell Biol* **20**, 102-112, doi:10.1016/j.tcb.2009.11.002 (2010).
- 34 Lee, B. J. & Mace, E. M. Acquisition of cell migration defines NK cell differentiation from hematopoietic stem cell precursors. *Mol Biol Cell* **28**, 3573-3581, doi:10.1091/mbc.E17-08-0508 (2017).

- 35 Wagner, T., Kroll, A., Haramagatti, C. R., Lipinski, H. G. & Wiemann, M. Classification and Segmentation of Nanoparticle Diffusion Trajectories in Cellular Micro Environments. *PLoS One* **12**, e0170165, doi:10.1371/journal.pone.0170165 (2017).
- 36 Lu, X., Kim-Han, J. S., Harmon, S., Sakiyama-Elbert, S. E. & O'Malley, K. L. The Parkinsonian mimetic, 6-OHDA, impairs axonal transport in dopaminergic axons. *Mol Neurodegener* **9**, 17, doi:10.1186/1750-1326-9-17 (2014).
- 37 Stepkowski, T. M., Meczynska-Wielgosz, S. & Kruszewski, M. mitoLUHMES: An Engineered Neuronal Cell Line for the Analysis of the Motility of Mitochondria. *Cell Mol Neurobiol* **37**, 1055-1066, doi:10.1007/s10571-016-0438-0 (2017).
- 38 Blum, D. *et al.* Molecular pathways involved in the neurotoxicity of 6-OHDA, dopamine and MPTP: contribution to the apoptotic theory in Parkinson's disease. *Prog Neurobiol* **65**, 135-172, doi:10.1016/s0301-0082(01)00003-x (2001).
- 39 Betarbet, R., Sherer, T. B. & Greenamyre, J. T. Animal models of Parkinson's disease. *Bioessays* **24**, 308-318, doi:10.1002/bies.10067 (2002).
- 40 Glinka, Y. Y. & Youdim, M. B. H. Inhibition of mitochondrial complexes I and IV by 6-hydroxydopamine. *European Journal of Pharmacology: Environmental Toxicology and Pharmacology* **292**, 329-332, doi:https://doi.org/10.1016/0926-6917(95)90040-3 (1995).
- 41 Patel, V. P., Defranco, D. B. & Chu, C. T. Altered transcription factor trafficking in oxidatively-stressed neuronal cells. *Biochim Biophys Acta* **1822**, 1773-1782, doi:10.1016/j.bbadis.2012.08.002 (2012).
- 42 Schuler, F. & Casida, J. E. Functional coupling of PSST and ND1 subunits in NADH:ubiquinone oxidoreductase established by photoaffinity labeling. *Biochim Biophys Acta* **1506**, 79-87, doi:10.1016/s0005-2728(01)00183-9 (2001).
- 43 Degli Esposti, M. Inhibitors of NADH-ubiquinone reductase: an overview. *Biochim Biophys Acta* **1364**, 222-235, doi:10.1016/s0005-2728(98)00029-2 (1998).
- 44 Lummen, P. Complex I inhibitors as insecticides and acaricides. *Biochim Biophys Acta* **1364**, 287-296, doi:10.1016/s0005-2728(98)00034-6 (1998).
- 45 Sanders, L. H. & Timothy Greenamyre, J. Oxidative damage to macromolecules in human Parkinson disease and the rotenone model. *Free Radic Biol Med* **62**, 111-120, doi:10.1016/j.freeradbiomed.2013.01.003 (2013).
- 46 Sherer, T. B. *et al.* Mechanism of toxicity in rotenone models of Parkinson's disease. *J Neurosci* **23**, 10756-10764 (2003).
- 47 Uversky, V. N. Neurotoxicant-induced animal models of Parkinson's disease: understanding the role of rotenone, maneb and paraquat in neurodegeneration. *Cell Tissue Res* **318**, 225-241, doi:10.1007/s00441-004-0937-z (2004).
- 48 Borland, M. K. *et al.* Chronic, low-dose rotenone reproduces Lewy neurites found in early stages of Parkinson's disease, reduces mitochondrial movement and slowly kills differentiated SH-SY5Y neural cells. *Mol Neurodegener* **3**, 21, doi:10.1186/1750-1326-3-21 (2008).
- 49 Jiang, Q., Yan, Z. & Feng, J. Neurotrophic factors stabilize microtubules and protect against rotenone toxicity on dopaminergic neurons. *J Biol Chem* **281**, 29391-29400, doi:10.1074/jbc.M602740200 (2006).
- 50 Ren, Y., Liu, W., Jiang, H., Jiang, Q. & Feng, J. Selective vulnerability of dopaminergic neurons to microtubule depolymerization. *J Biol Chem* **280**, 34105-34112, doi:10.1074/jbc.M503483200 (2005).
- 51 Srivastava, A. S. *et al.* Embryonic stem cells ameliorate piroxicam-induced colitis in IL10-/- KO mice. *Biochem Biophys Res Commun* **361**, 953-959, doi:10.1016/j.bbrc.2007.07.139 (2007).
- 52 Simoes, R. F. *et al.* Refinement of a differentiation protocol using neuroblastoma SH-SY5Y cells for use in neurotoxicology research. *Food Chem Toxicol* **149**, 111967, doi:10.1016/j.fct.2021.111967 (2021).

- 53 Kandel, J., Chou, P. & Eckmann, D. M. Automated detection of whole-cell mitochondrial motility and its dependence on cytoarchitectural integrity. *Biotechnol Bioeng* **112**, 1395-1405, doi:10.1002/bit.25563 (2015).
- 54 trajpy v. 1.3.1 (Zenode, 2020).
- 55 Moreira-Soares, M., Cunha, S. P., Bordin, J. R. & Travasso, R. D. M. Adhesion modulates cell morphology and migration within dense fibrous networks. *Journal of Physics: Condensed Matter* **32**, 314001, doi:10.1088/1361-648x/ab7c17 (2020).
- 56 Theodorou, D. N. & Suter, U. W. Shape of unperturbed linear polymers: polypropylene. *Macromolecules* **18**, 1206-1214, doi:10.1021/ma00148a028 (1985).
- 57 Arkin, H. & Janke, W. Gyration tensor based analysis of the shapes of polymer chains in an attractive spherical cage. *J Chem Phys* **138**, 054904, doi:10.1063/1.4788616 (2013).
- 58 Helmuth, J. A., Burckhardt, C. J., Koumoutsakos, P., Greber, U. F. & Sbalzarini, I. F. A novel supervised trajectory segmentation algorithm identifies distinct types of human adenovirus motion in host cells. *J Struct Biol* **159**, 347-358, doi:10.1016/j.jsb.2007.04.003 (2007).

## Acknowledgements

This work was funded by Montepio Foundation and FEDER/COMPETE/national funds by FCT under research grants PTDC/BTM-SAL/29297/2017, POCI-01-0145-FEDER-029297 (MitoScreening), UIDB/04539/2020 (CNC Strategic Plan), PTDC/MED-FAR/29391/2017, POCI-01-0145-FEDER-029391 (Mito4ALS), UIDB/04564/2020. R.F. Simões (PD/BD/128254/2016) was supported by ERDF through COMPETE 2020/FCT. T.C.O was supported by DL57/2016/CP1448/CT0016. JN was supported in part by the grant 21-04607X from the Czech Science Foundation. M. M-S was supported by European Union's Horizon 2020 research and innovation programme under the Marie Skłodowska-Curie grant agreement No 801133.

## Author contributions

All authors conceived and designed the study. R.F.S and J.K. performed the experiments and did investigation. R.F.S, M.M.S and R.P. formed the methodology. T.C.O., P.J.O and J.N. found resources required. R.F.S, M.M.P and R.P. wrote the paper. R.F.S., R.P., M.M.S., J.N., R.T., P.J.O., T.C.O. and F.B.P. reviewed and edited the manuscript. All authors read and approved the manuscript.

## **Additional information**

### **Competing Interests Statement**

The authors declare no competing of interest.

# Figures

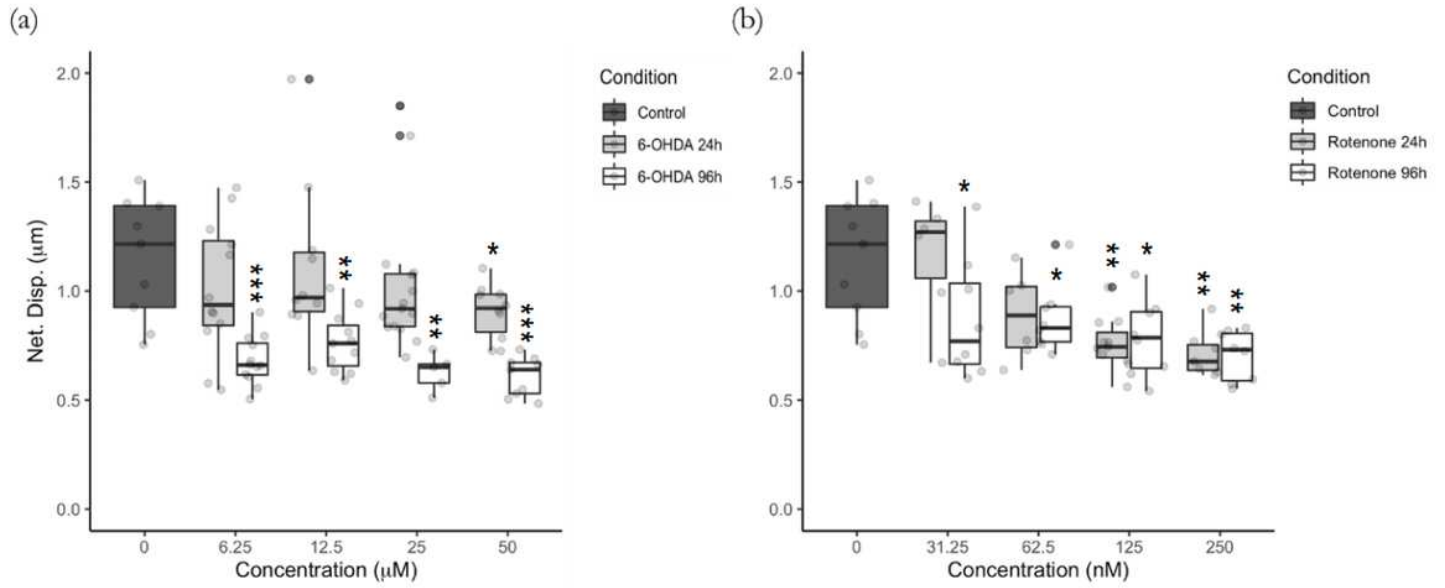


**Figure 1**

6-OHDA (a) and rotenone (b) reduced mitochondrial net displacement. Mitochondria were labeled with the fluorescent dye MitoTracker Red CMXRos, their movement followed, and trajectory net displacement was calculated as stated in Materials and Methods. Data are presented as boxplots, in which each dot represents the mean of each mitochondrial movement per video frame (n=5 to 15). Kruskal-Wallis test (one-way ANOVA on ranks) pair-wise (control vs 6-OHDA or control vs rotenone) was used to assess statistical significance, (\*\*\*)  $p < 0.001$  (\*\*),  $p < 0.01$ , (\*)  $p < 0.05$ .

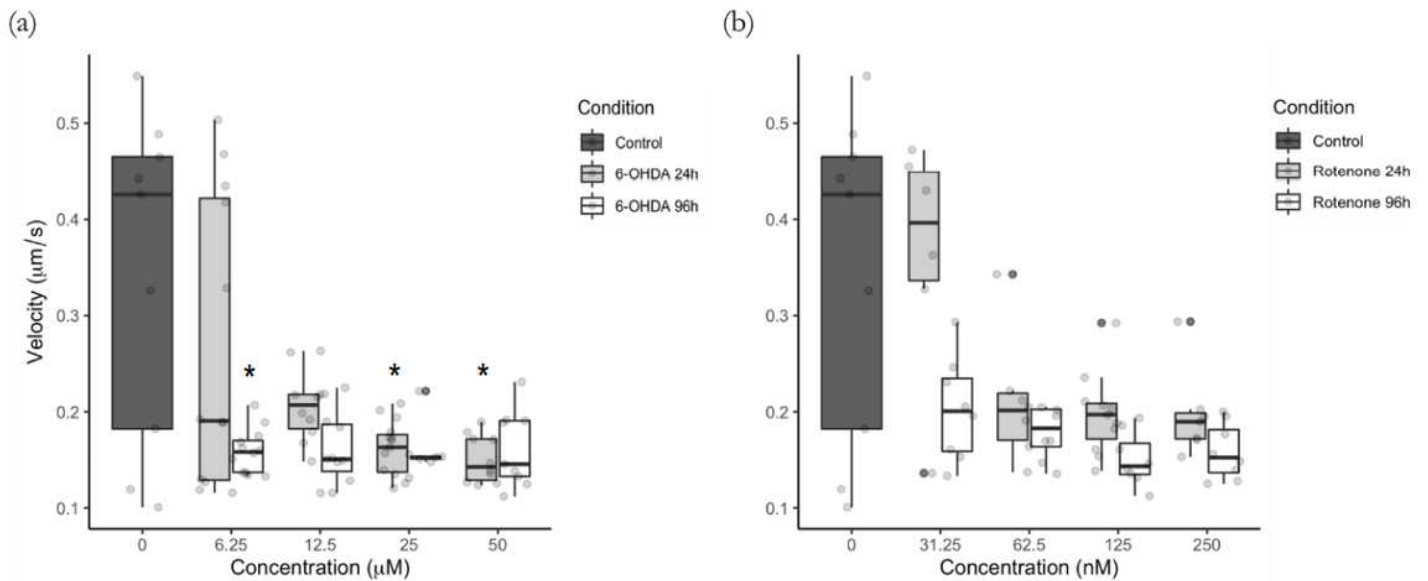


**Figure 2**

Mitochondrial mean velocity is lower due to 6-OHDA (a) and rotenone (b) treatment. Mitochondria were labeled with the fluorescent dye MitoTracker Red CMXRos, their movement followed, and trajectory mean velocity was calculated as stated in Materials and Methods. Data are presented as boxplots in which each dot represents the mean of each mitochondrial movement per video frame (n=5 to 15). Kruskal-Wallis test (One-way ANOVA on ranks) pair-wise (control vs 6-OHDA or control vs rotenone) was used to assess statistical significance, (\*)  $p < 0.05$ .

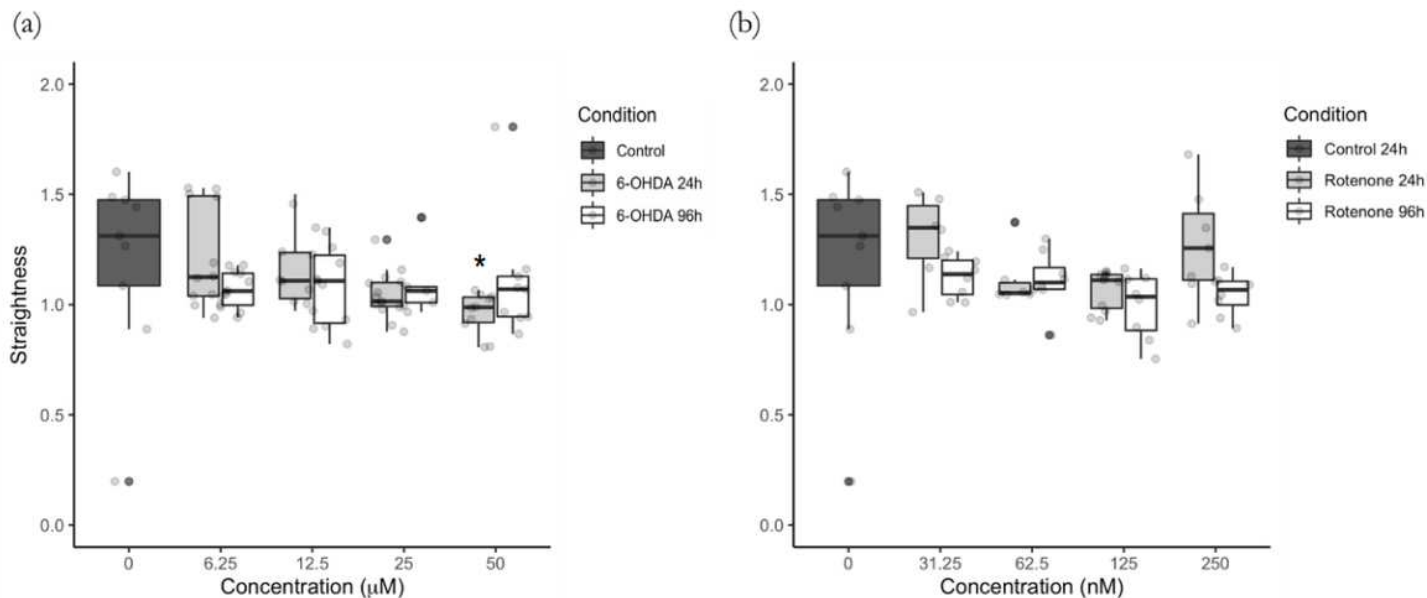


**Figure 3**

Mitochondrial movement pattern straightness was affected in cells treated with 6-OHDA (a) and rotenone (b). Mitochondria were labeled with the fluorescent dye MitoTracker Red CMXRos, their movement followed, and trajectory straightness was calculated as stated in Materials and Methods. Data are presented as boxplots in which each dot represents the mean of each mitochondria movement per video frame (n=5 to 15). Kruskal-Wallis test (One-way ANOVA on ranks) pair-wise (control vs 6-OHDA or control vs rotenone) was used to assess statistical significance, (\*)  $p < 0.05$ .



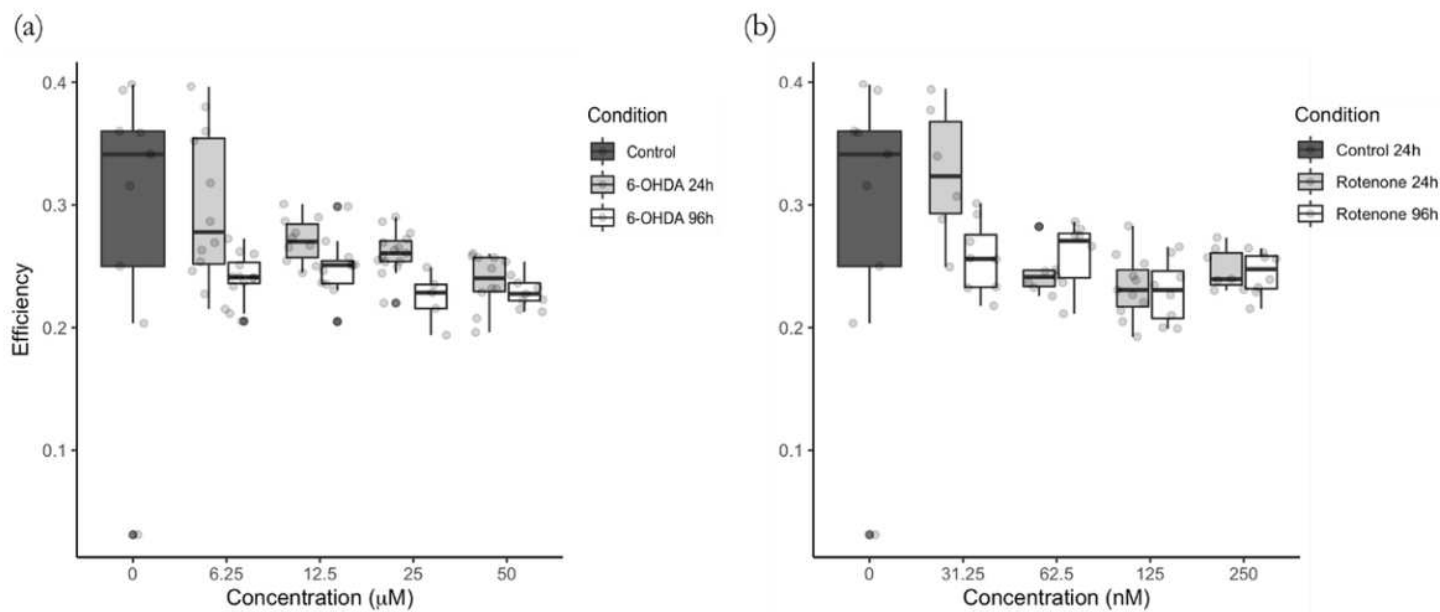


**Figure 4**

Mitochondrial trajectory efficiency was decreased in cells treated with 6-OHDA (a) and with rotenone (b). Mitochondria were labeled with the fluorescent dye MitoTracker Red CMXRos, their movement followed, and trajectory efficiency was calculated as stated in Materials and Methods. Data are represented as boxplots in which each dot represents the mean of each mitochondria movement per video frame ( $n=5$  to 15). Kruskal-Wallis test (One-way ANOVA on ranks) pair-wise (control vs 6-OHDA or control vs rotenone) was used to assess statistical significance.

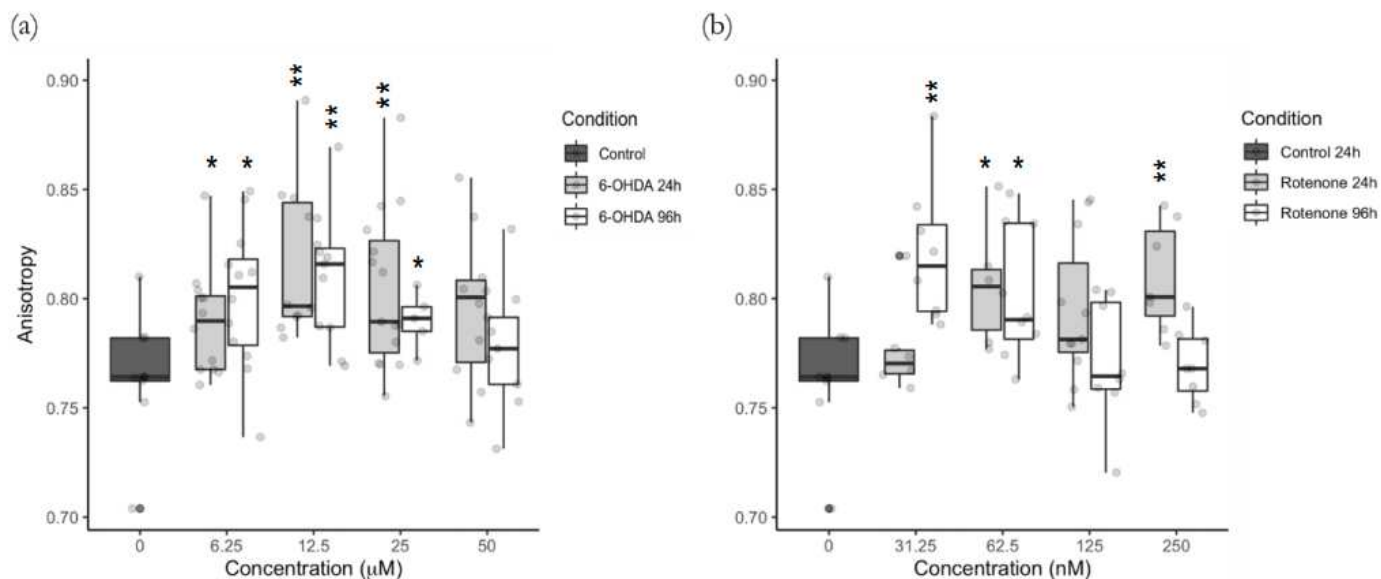


**Figure 5**

6-OHDA (a) and rotenone (b) promote higher degree of mitochondrial movement anisotropy. Mitochondria were labeled with the fluorescent dye MitoTracker Red CMXRos, their movement followed,

and trajectory anisotropy was calculated as stated in Materials and Methods. Data are represented as boxplots in which each dot represents the mean of each mitochondria movement per video frame (n=5 to 15). Kruskal-Wallis test (One-way ANOVA on ranks) pair-wise (control vs 6-OHDA or control vs rotenone) was used to assess statistical significance, (\*\*),  $p < 0.01$ , (\*)  $p < 0.05$ .

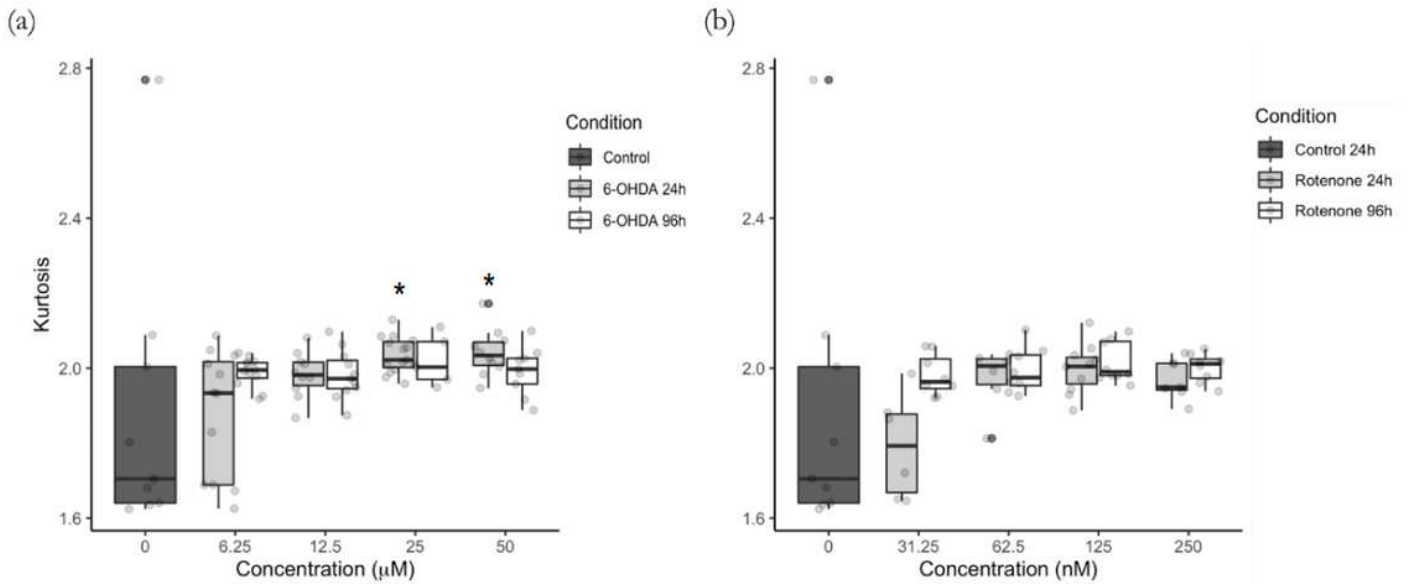


**Figure 6**

Kurtosis of mitochondrial movement and the effect of 6-OHDA (a) and rotenone (b). Mitochondria were labeled with the fluorescent dye MitoTracker Red CMXRos, their movement followed, and trajectory kurtosis was calculated as stated in Materials and Methods. Data are represented as boxplots in which each dot represents the mean of each mitochondria movement per video frame (n=5 to 15). Kruskal-Wallis test (One-way ANOVA on ranks) pair-wise (control vs 6-OHDA or control vs rotenone) was used to assess statistical significance, (\*)  $p < 0.05$ .

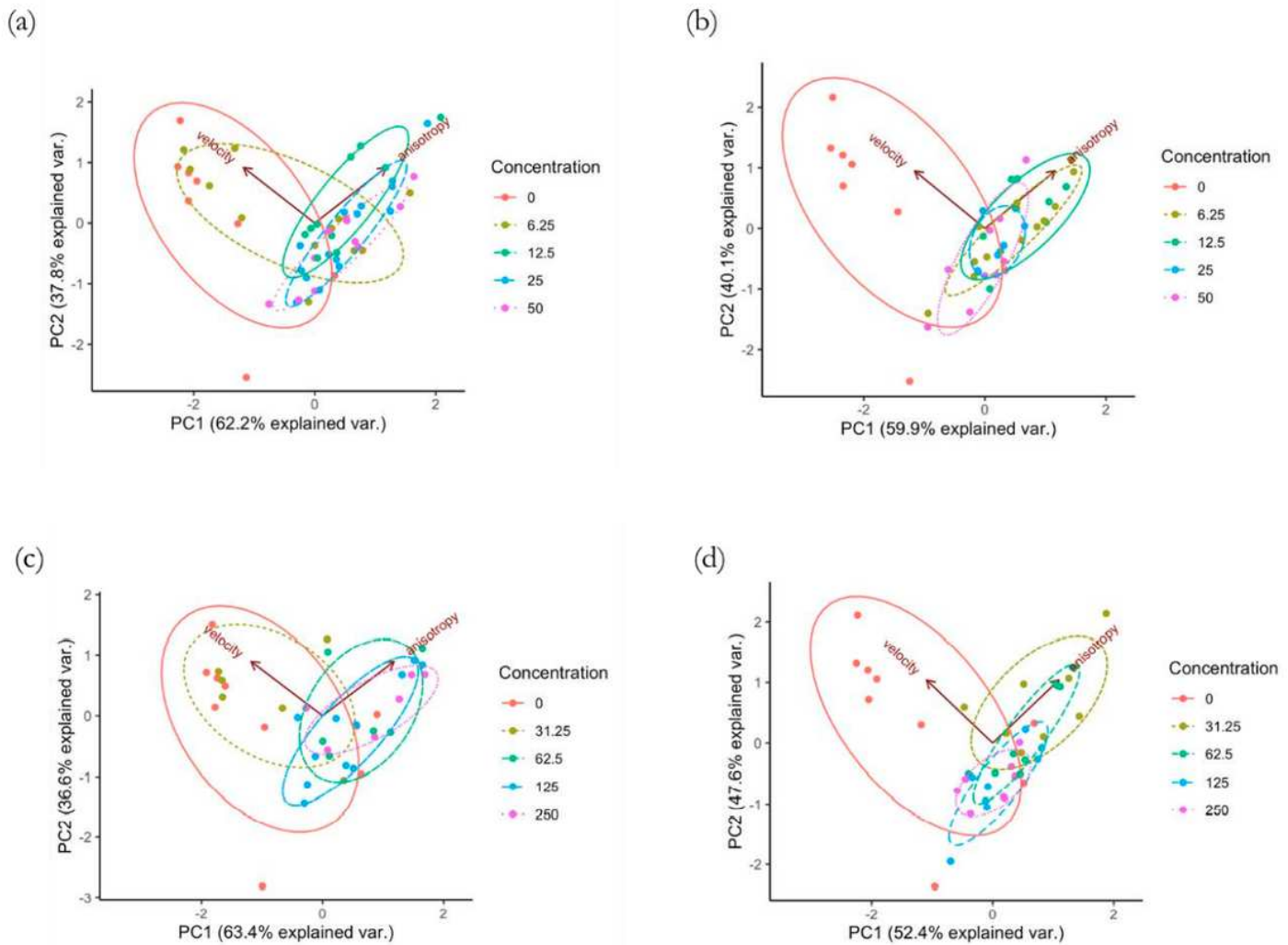


**Figure 7**

The panel shows PCAs for control together with each different treatment: 6-OHDA for 24 h (a) and 96 h (b) and rotenone for 24 h (c) and 96 h (d). The normal data ellipses are superposed. Only the two best features that better distinguish between the treatments and control conditions were considered, i.e. velocity and anisotropy. In general, the treatments grouped far from the control and presented higher variance along the anisotropy direction, apart from the treatments for 24 h with lowest concentration of 6-OHDA and rotenone.

## Supplementary Files

This is a list of supplementary files associated with this preprint. Click to download.

- [SupplementaryMethods.docx](#)
- [Supplementaryfiguresonline.docx](#)